This is the post-print (i.e. final draft post-refereeing) of the publication.
The final publication is available at Elsevier via http://dx.doi.org/10.1016/j.jallcom.2018.10.060

Assessment of the functional properties stability in $(Ba_{0.85}Ca_{0.15})(Zr_{0.1}Ti_{0.9})O_3$ piezoceramics: Huge dielectric and piezoelectric nonlinearity

Diego A. Ochoa,[1] Armando Reyes-Montero,[2] Francesc Suñol,[1] Maria E. Villafuerte-Castrejón,[2] Lorena Pardo,[3] and Jose E. García[1,*]

[1] *Department of Physics, Universitat Politècnica de Catalunya - BarcelonaTech, 08034 Barcelona, Spain.*

[2] *Instituto de Investigaciones en Materiales, Universidad Nacional Autónoma de México, Ciudad Universitaria, A.P. 70-360, C.P. 04510 CDMX, Mexico.*

[3] *Instituto de Ciencia de Materiales de Madrid, CSIC, c/Sor Juana Inés de la Cruz 3, Cantoblanco, 28049 Madrid, Spain.*

Abstract

The (Ba,Ca)(Zr,Ti)O_3 ceramic system has received special attention in recent years because it may lead to promising lead-free piezoceramics. However, the stability of the functional properties of these materials is an important issue that requires greater attention. In this work, the $(Ba_{0.85}Ca_{0.15})(Zr_{0.1}Ti_{0.9})O_3$ compound (BCZT) is taken as a reference material for evaluating the variation of the functional properties when an external stimulus (e.g., electric field or dynamical stress) is applied, which may constitute an important drawback of piezoceramics. The results show that BCZT exhibits a huge nonlinear behavior, which notably limits this lead-free material for transfer to applications. The instabilities manifest at considerably low amplitudes of the applied electric field or dynamical stress due to a large extrinsic contribution from the irreversible motion of domain walls. Understanding and controlling the physical phenomena related to the domain wall motion presents a fundamental challenge for achieving an effective enhancement of the functional property stability of this system.

Keywords: BCZT; Lead-free piezoceramics; Nonlinear response; Property stability; Rayleigh analysis.

* Corresponding author.
E-mail address: jose.eduardo.garcia@upc.edu (J.E. García).

This is the post-print (i.e. final draft post-refereeing) of the publication.
The final publication is available at Elsevier via http://dx.doi.org/10.1016/j.jallcom.2018.10.060

1. Introduction

Research in lead-free materials has been motivated by the necessity to expel lead-containing devices from the commercial applications. The toxicity effects of lead and lead oxide are well known. Due to the absorption from the lungs, skin or the gastrointestinal system, lead may be incorporated into the human body, resulting in severe damage to the blood, the gastrointestinal and neurological systems, thereby compromising human health [1]. Toxicity and environmental issues are the main reason why lead has been banned from many commercial applications such as fuel, paint, solders, food-processing equipment, plumbing and lubricating greases. In the field of piezoelectric materials, research into lead-free piezoelectrics has been strongly triggered by legislation introduced for restricting the use of certain hazardous substances, including lead, in electrical and electronic equipment.

Replacing lead-containing piezoelectric materials has become one of the crucial challenges in materials science since the research by Saito et. al. [2] was published. Studies have mainly been focused on the substitution of $Pb(Zr,Ti)O_3$ (PZT) system as the most commonly used piezoelectric material in commercial applications. Promising candidates like $(K,Na)NbO_3$ (KNN)- and $(Bi_{0.5}Na_{0.5})TiO_3$-$BaTiO_3$ (BNT-BT)-based systems have for years been the object of study [3-5]. Similar to PZT, the KNN and BNT-BT systems show morphotropic phase boundary (MPB), which is at the core of the excellent piezoelectric functional properties of these systems. However, unlike PZT, for which the MPB ends at a tricritical point where rhombohedral, tetragonal and cubic phases meet, the MPB of KNN and BNT-BT systems do not end at a tricritical point. The flattening of the energy profile near to the tricritical point enhances the intrinsic contribution by favoring the polarization reorientation (polarization rotation) as well as the polarization extension [6]. In addition, the extrinsic contribution, and in particular the contribution related to domain walls motion, also increase near the MPB [7], as occurs in PZT, where this contribution may account for 70% of the total material response at room temperature [8,9].

A promising lead-free system that also presents MPB ending at a tricritical point is the $Ba(Zr,Ti)O_3$-$(Ba,Ca)TiO_3$ system [10]. The first report of the high longitudinal piezoelectric coefficient (d_{33}~620 pC/N) and the large signal piezoelectric coefficient (d^*_{33}=1140 pm/V) of this system [11] again revolutionized research into lead-free piezoelectrics. The study focused on the $Ba(Zr_{0.2}Ti_{0.8})O_3$-$x(Ba_{0.7}Ca_{0.3})TiO_3$ compounds, where x is the molar percent of BCT. The MPB was found for x=50% at room temperature. Thus, the $(Ba_{0.85}Ca_{0.15})(Zr_{0.1}Ti_{0.9})O_3$ composition exhibits excellent functional properties that make this material one of the best

candidates for PZT replacement. Unfortunately, the low Curie temperature (T_C~360 K) of this system limits its working range. Furthermore, this system shows large temperature-dependence of functional properties, which is an important drawback for real applications. The curved MPB that appears in the phase diagram [12] provokes temperature-driven property instability. Small shifts in composition or temperature give rise to a substantial decrease in the piezoelectric coefficient, among other functional properties [13]. Notwithstanding these drawbacks, the system remains as a promising substitute of the PZT for sensor and actuator applications at room temperature, such as ultrasonic cleaners, ultrasonic machine tool, and nano-motors, among other [5].

The enhancement of the functional properties near MPBs in piezoelectric materials is a well-documented fact [14-16]. Both the intrinsic contribution, related to the field-induced lattice distortion (polarization rotation and extension) and the extrinsic contributions, related to the non-180° domain wall motion, maximize at the MPB. However, the nonlinear dielectric and piezoelectric responses also increase at the MPB [7]. The nonlinear behavior, understood as the variation of the functional properties when an external stimulus is applied (e.g., electric field or dynamical stress), is an undesirable phenomenon typically associated with domain wall motion [9]. Unfortunately, a recent study proves that the major contribution to the large piezoelectric response of $Ba(Zr,Ti)O_3$-$(Ba,Ca)TiO_3$ system is due to domain walls motion [17]. Consequently, this system is expected to show a notable nonlinear response.

The reliability and stability of the functional properties of lead-free piezoceramics are essential features for a successful PZT replacement. Hence, the stability of the functional properties of $(Ba_{0.85}Ca_{0.15})(Zr_{0.1}Ti_{0.9})O_3$ (hereafter labeled as BCZT) is explored in this work. The study is conducted on this composition since, as mentioned above, it is the most interesting composition of the $Ba(Zr,Ti)O_3$-$(Ba,Ca)TiO_3$ system from both the fundamental and practical points of view. The results show that BCZT exhibits a huge nonlinear behavior which notably limits the transfer of this lead-free material to applications. Note that the nonlinear behavior is associated with large dielectric and mechanical losses, which implies that the material easily overheats when it works as an active element of a piezoelectric transducer, particularly in actuator mode. Some functional properties of two well-known piezoceramics compositions are used for comparison purposes; that is, $(K_{0.44}Na_{0.52}Li_{0.04})(Nb_{0.86}Ta_{0.10}Sb_{0.04})O_3$ (hereafter labeled as KNL-NTS), which is one of the $(K,Na)NbO_3$-based materials with the best performance [2], and $Pb(Zr_{0.53}Ti_{0.47})O_3$ + 1 wt % Nb_2O_5 (hereafter labeled as PNZT), which is a representative soft-PZT material [9]. A traditional hard PZT piezoceramics and a promising single crystal, such as PZT8 [18] and PMN-PT [19], could also be used for comparison purposes. However,

it is well-known that hard piezoceramics exhibit a moderate nonlinear response [9] while the comparison between ceramics and single crystals turns out to be unequal.

2. Experimental

2.1. Samples preparation, structure and microstructure

BCZT ceramics were prepared by conventional solid-state method, as reported elsewhere [20]. $BaCO_3$ (99.0%, Analytica), $CaCO_3$ (99.0%, Fluka), TiO_2 (99.0%, Aldrich) and ZrO_2 (99.0%, Riedel-deHaën) were used as starting materials. Stoichiometric amounts of reagents were weighed and mixed with acetone for 30 min. They were then calcined at 1250 °C for 2 h. Afterwards, powders were ball milled for 24 h with zirconia ball media and alcohol, uniaxially pressed into ~13.0 mm diameter and ~1.5 mm thickness pellets, and then sintered at 1400 °C for 2 h in air. Details about the synthesis method and fundamental characterization of PNZT and KNL-NTS ceramics can be found elsewhere [9,21].

The phase structure of BCZT was examined by X-ray diffraction (XRD) measurements using a Bruker-D8 Advance diffractometer (Cu-Kα radiation, λ= 1.5406 Å) at room temperature. The data was collected from 20 to 120° (2θ) with 40 kV and 40 mA, step= 0.02° and 5 s integration time. Fig. 1 shows the XRD patterns of BCZT bulk ceramic, revealing a single perovskite phase structure. The wide $\{200\}_{pc}$ peak broadening shown at the magnified angle in the 2θ range 44-46º is attributed to the coexistence of the rhombohedral and tetragonal crystallographic phases [22]. This result is in agreement with previously reported literature [11] in which the peak overlapping reveals symmetries coexistence at the MPB composition.

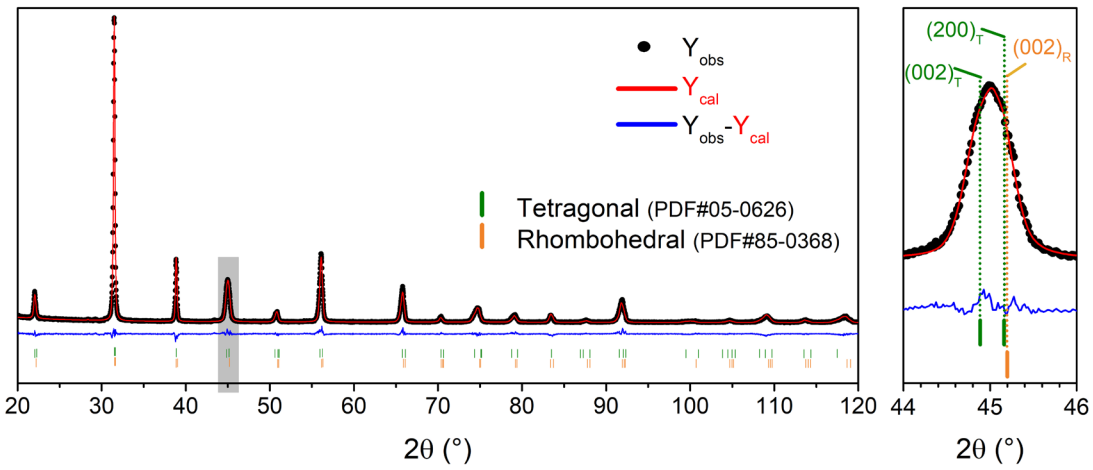

Fig. 1. Rietveld refinement of the X-ray diffraction patterns of BCZT ceramics. Magnification between 44° and 46° (2θ) of the XRD patterns is also shown.

TOPAS software was used to carry out a Rietveld analysis, which was performed by assuming a MPB composition based on the coexistence of rhombohedral (*R3m*) and tetragonal (*P4mm*) ferroelectric phases. The main characteristics of the structural refinement (lattice parameters, cell volume, the average crystal strain and the percentage of each ferroelectric phase) are shown in Table 1. The space groups of $BaTiO_3$ for rhombohedral and tetragonal phases were used as initial conditions for the refinement, resulting in a good fit to the experimental data (i.e. a quality factor R_{wp}= 9.826). The Rietveld analysis shows that, as expected, there is a similar fraction of rhombohedral and tetragonal phases for the studied composition.

Table 1. Phase fraction and lattice parameters obtained from Rietveld refinement of the X-ray diffraction data of BCZT ceramics, using a tetragonal (*P4mm*) and rhombohedral (*R3m*) phase coexistence model.

Crystal system	Phase fraction (%)	Lattice parameters		Volume (Å^3)	Avg. strain
		a=b (Å)	c (Å)		
Rhombohedral	45	4.0087(2)	4.0087(2)	64.4201	0.2144(2)
Tetragonal	55	4.0377(1)	4.0217(2)	65.5664	0.5317(1)

The size and morphology of grain of sintered samples were analyzed using a Jeol 7600F field emission scanning electron microscope (FE-SEM). Fig. 2 shows the FE-SEM results from the surface of the sample, revealing a highly dense microstructure (~97%). The average grain size of a large sample area was determined by the interception method. An estimated average grain size of 18.2 µm with a standard deviation of 4.6 µm was obtained.

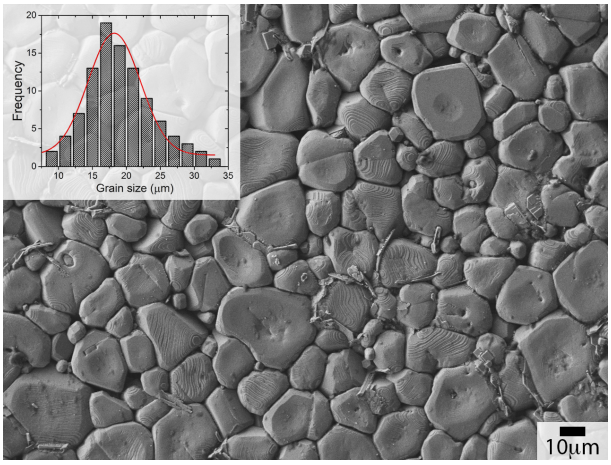

Fig. 2. FE-SEM micrograph showing dense BCZT ceramics. The grain size distribution (GSD) histogram is also shown.

2.2. Measurement methods

The dielectric and piezoelectric characterizations as a function of the temperature were performed using a closed-loop cryogenic system consisting of a helium compressor (Cryogenics 8200), a cold finger (Cryogenic model 22), and a vacuum pump (Alcatel Drytel Micro CFV100D). The system allows sweeping in a temperature range from 30 K to 390 K by using a temperature controller (LakeShore model 331). The dielectric characterization was performed in unpoled samples using an Agilent E4980A Precision LCR Meter, the real ε' and imaginary ε'' parts of the permittivity being measured at several frequencies between 100 Hz and 1 MHz. The piezoelectric characterization was performed in accordance with the standards of measurements [23] in poled ceramics using an impedance analyzer (HP4294A, Agilent Technologies Inc., Santa Clara, CA). Resonance and anti-resonance frequencies of the first extensional mode of a thickness poled thin bar, as well as the capacitance value at a frequency where the motional admittance is null, were measured in order to obtain the elastic and piezoelectric coefficients. Using the measured variables and the exact solution for the admittance of the length-extensional resonance of a thickness poled thin bar with thickness excitation enables the compliance (s_{11}^{E}), the electromechanical coupling factor (k_{31}), the piezoelectric coefficient (d_{31}), and the dielectric permittivity (ε_{33}^{T}) of the poled samples to be obtained. A detailed description of the method employed can be found elsewhere [24].

The nonlinear dielectric characterization was performed at room temperature by applying a sub-switching ac electric field at 1 kHz. A capacitance comparator bridge specially designed for this type of measurement was used to conduct the experiment [25]. The direct nonlinear piezoelectric characterization was performed using a Berlincourt-type method at room temperature. Sinusoidal stress superimposed onto a constant compression force was applied to the samples. The value of the applied uniaxial compression stress was kept below 40 MPa in order to prevent irreversible depolarization of the samples. An extended description of these measurements can be found elsewhere [26].

3. Results and discussion

3.1. Temperature dependence of macroscopic properties

Fig. 3 shows the temperature dependence of the real and imaginary parts of the relative permittivity. As may be observed, the ferroelectric to paraelectric phase transition occurs at a relatively low Curie temperature (T_C~360K), as expected. Furthermore, the dielectric anomaly related to the rhombohedral-to-tetragonal phase transition appears slightly above room

temperature, which is similar to that in previous works [11,27]. The inset of Fig. 3(a) shows the dielectric response at very low temperatures. The decrease in the dielectric response at low temperatures is a typical behavior of piezoelectric materials and has been observed in PNZT [24] and KNL-NTS [28]. The values reported in this work are similar to the values for KNL-NTS and slightly lower than PNZT. Since the response at low temperatures is due only to the intrinsic contribution (when $T\rightarrow 0$ K the domain wall motion freezes), it is possible to affirm that the intrinsic response of BCZT is similar to the previously studied KNL-NTS lead-free composition. At room temperature, however, where both compositions show coexistence of ferroelectric phases, the $\varepsilon'_{BZT-BCT} = 2850$ is more than twice the $\varepsilon'_{KNL-NTS} = 1100$. In the BCZT compound, the rhombohedral crystallographic phase, with polarization vector $P^R = (P_1^R, P_1^R, P_1^R)$ along the pseudo-cubic direction $[111]_C$ and eight possible directions of polarization, coexists with the tetragonal crystallographic phase, with polarization vector $P^T = (0,0, P_3^C)$ along the pseudo-cubic direction $[001]_C$ with six possible directions of polarization. The ferroelectric phase coexistence at the MPB could enhance the polarization rotation. Therefore, the polarization rotation could be the cause of the large dielectric coefficient value near room temperature. However, this reasoning does not explain the higher value of the dielectric constant of BCZT as compared with KNL-NTS. The two crystallographic phases coexisting in KNL-NTS at room temperature may also enhance the polarization rotation. The orthorhombic crystallographic phase, with $P^O = (P_1^O, 0, P_1^O)$ along the $[111]_C$ pseudo-cubic direction and twelve possible directions of polarization, together with the tetragonal crystallographic phases, add a total of eighteen possible directions of polarization. From this perspective, the increase in the intrinsic contribution through polarization extension and the increase in the extrinsic contribution related to domain walls motion should be taken into consideration, as has been previously reported [17]. Finally, the higher dielectric constant in BCZT proves that the free-energy density profile of this system is more flattened than that of the KNL-NTS as a result of the existence of the tricritical point in the BCZT system.

This is the post-print (i.e. final draft post-refereeing) of the publication.
The final publication is available at Elsevier via http://dx.doi.org/10.1016/j.jallcom.2018.10.060

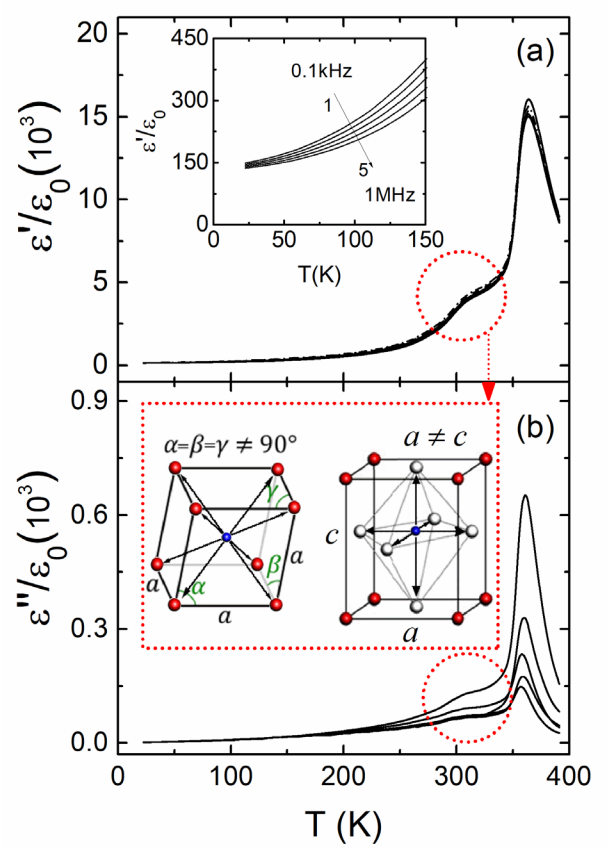

Fig. 3. Real (a) and imaginary (b) parts of the relative permittivity versus temperature of BCZT, from very low temperatures until above the ferroelectric-to-paraelectric phase transition, at several frequencies from 0.1 kHz to 1 MHz. The insets in (a) show a zoom of the low-temperature region for real permittivity. The dotted circles show a dielectric anomaly that is related to the rhombohedral-to-tetragonal phase transition. The inset in (b) shows a schematic representation of the symmetries coexisting in the polymorphic region.

The behavior of the imaginary part of the permittivity (dielectric losses) is similar to the real part. Since the domain wall motion freezes at low temperature ($T \rightarrow 0$ K), the intrinsic dielectric loss mechanisms should be the same for both BCZT and KNL-NTS compositions; i.e., $\varepsilon''_{BCZT} \approx \varepsilon''_{KNL-NTS} \approx 0$, as expected. However, at room temperature, the value of $\varepsilon''_{BZT-BCT} = 60$ doubles the value of $\varepsilon''_{KNL-NTS} = 30$. The high dielectric losses of the BCZT could be associated with intrinsic and extrinsic phenomena. The polarization rotation of the unit cell links with energy dissipation due to the energy barrier that is overcome to switch the polarization vector [29] (intrinsic dielectric loss). On the other hand, the domain wall motion through a defects field always generates dielectric losses [30]. In any case, previous results [17] demonstrated that domain wall motion is the dominant contribution to BCZT functional response.

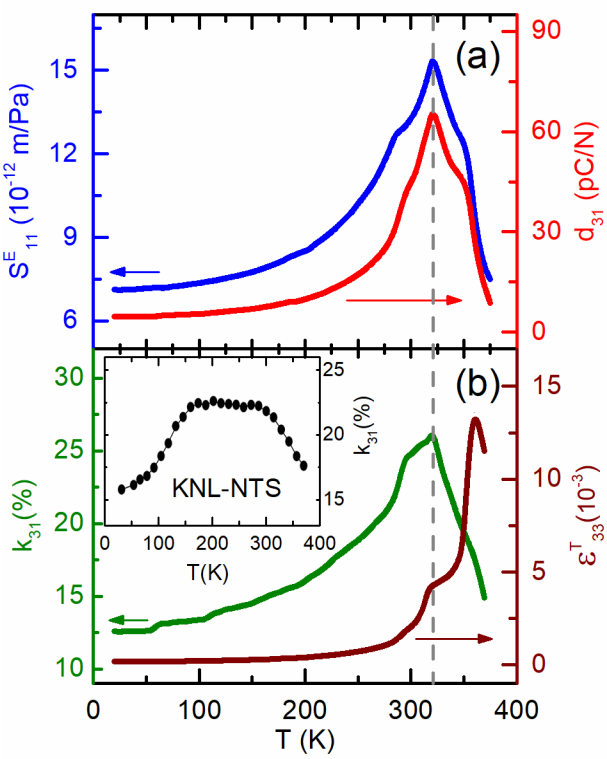

Fig. 4. Temperature dependence of the compliance s_{11}^E (a), piezoelectric coefficient d_{31} (a), electromechanical coupling factor k_{31} (b) and dielectric constant ε_{33}^T (b) in a poled BCZT sample. The inset in panel (b) shows the temperature dependence of the electromechanical coupling factor for KNL-NTS piezoceramics that is used for comparison purpose.

Given that the BCZT may be interesting for its use in piezoelectric applications, the mechanical and piezoelectric behavior must also be analyzed. Fig. 4 shows the temperature dependence of the mechanical, piezoelectric, dielectric, and coupling factor coefficients of this compound. The low temperature values of all coefficients are similar to KNL-NTS values [28], thereby confirming that the intrinsic contribution of the KNL-NTS and BCZT systems can be considered the same. All the coefficients increase monotonically from low temperature values to maximum values above room temperature. The compliance (s_{11}^E), the piezoelectric coefficient (d_{31}) and the electromechanical coupling factor (k_{31}) show their maximum values at the same temperature (~320 K), which matches with the anomaly on the dielectric permittivity related to the ferroelectric-to-ferroelectric phase transition. This behavior proves the enhancement of the functional properties at the MPB, and validates BCZT as a promising lead-free composition. Moreover, the BCZT electromechanical coupling factor is 5% higher than the k_{31} of KNL-NTS at room temperature. Despite the high value of electromechanical coupling factor, $k_{31}^{BCZT} = 27\%$, it exhibits a significant drawback. While the maximum for the k_{31} coefficient in KNL-NTS exhibits a flat region near room temperature (inset of Fig. 4(b)),

the k_{31} of BCZT shows a sharp maximum with significant k_{31}variations for small temperature deviations (Fig. 4(b)).

The temperature stability of the functional properties is as important as all the other physical properties. The narrow peak around the maximum value existing in all the coefficients of BCZT thus constitutes a critical disadvantage as reagrds the KNL-NTS. As a consequence, small temperature variations lead to considerable decreases in the BCZT functional properties. For instance, the d_{31} coefficient drops by 10% of the maximum value at a 5 K shift of temperature, thereby restricting the use of BCZT compound in practical applications. The narrow peak in all the coefficients of BCZT may be related to the closeness between the ferroelectric-to-ferroelectric and the ferroelectric-to-paraelectric phase transitions. Both phase transitions occur with only ΔT= 60 K of difference, thus sharpening the decrease in functional properties just after the ferroelectric-to-ferroelectric phase transition. The phase transitions of KNL-NTS are separated by ΔT= 250 K, which may favor the appearance of the flat region in the functional properties. The extremely curved MPB of the BCZT system could also be responsible for the temperature instability of the functional properties.

3.2. Nonlinear response

Dielectric nonlinearity in BCZT under a bias (DC) electric field has recently been reported in regard to the energy storage utilization [31]. Here, we show the nonlinear dielectric response as the variation of the real and imaginary parts of the permittivity with the amplitude of the applied alternating electric field (Fig. 5(a)). The nonlinear dielectric response of KNL-NTS and PNZT has been added for comparison purposes. As may be observed, the BCZT shows a colossal nonlinear dielectric behavior, incrementing the variation of the real part of the relative permittivity by 2500 at a relatively low amplitude of the electric field; i.e., $\Delta\varepsilon'$= 2500 at E_0= 0.1 MV/m. Moreover, the variation of the imaginary part is enormously high ($\Delta\varepsilon''$= 1300 at E_0=0.1 MV/m) when compared with the typical values in other piezoelectric materials [9,28]. On comparison with BCZT for the same E_0, both KNL-NTS and PNZT show little variation in dielectric constant. The observed behavior of the permittivity of the BCZT demonstrates a notable instability of the dielectric properties with the amplitude of the applied electric field; i.e. large nonlinear dielectric response.

This is the post-print (i.e. final draft post-refereeing) of the publication.
The final publication is available at Elsevier via http://dx.doi.org/10.1016/j.jallcom.2018.10.060

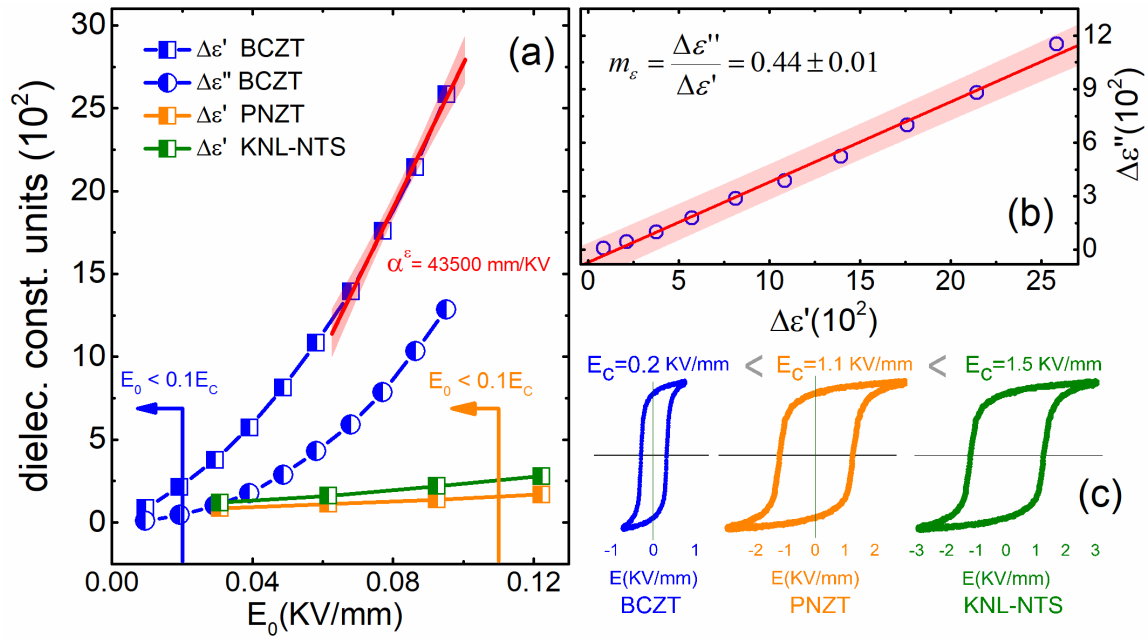

Fig. 5. Nonlinear dielectric response at 1 kHz and at room temperature. The increments of the real and the imaginary parts of the relative permittivity as a function of the applied ac electric field amplitude are shown in panel (a) for BCZT. The increments of the real relative permittivity for KNL-NTS and PNZT are also shown for comparison purposes. The relation between the increments of the real and imaginary permittivity is displayed in panel (b). The panel (c) shows the ferroelectric hysteresis loop for BCZT, PNZT and KNL-NTS.

Another differentiated feature of BCZT is the nonlinear dependence of $\Delta\varepsilon'$ and $\Delta\varepsilon''$with E_0. Typically, soft piezoelectric materials, such as KNL-NTS and PNZT, exhibit a linear dependence of $\Delta\varepsilon'$ and $\Delta\varepsilon''$with E_0 that could be described by the Rayleigh model [30,32]. According to this model, the nonlinear response is governed by a linear dependence of the real and imaginary parts of the permittivity with the amplitude of the applied electric field, as in [32]:

$$\varepsilon' = \varepsilon_0(\varepsilon_L + \alpha^\varepsilon E_0),$$
$$\varepsilon'' = \varepsilon_0(\frac{4}{3\pi}\alpha^\varepsilon E_0),$$

where ε_L is the value of the dielectric coefficient at zero-field amplitude, and α^ε is the Rayleigh coefficient that quantifies the nonlinear dielectric response. For $\alpha^\varepsilon = 0$, no dependence of the permittivity with E_0 there exist, thereby denoting a linear and stable dielectric response. Thus, at higher values of α^ε a higher nonlinear dielectric response is displayed. Furthermore, the relation between the increments of the real and imaginary part of the permittivity, $m_\varepsilon = \frac{\Delta\varepsilon''}{\Delta\varepsilon'} = 0.42$, is a constant value. In the framework of Rayleigh model, an increment in the dielectric

constant necessarily involves a certain increment in the dielectric losses. The model assumes that the nonlinear behavior, understood as the permittivity increment, is related to the irreversible motion of the domain walls in a random pinning centers field [30].

Although the BCZT do not fulfill the Rayleigh model, analysis of the nonlinear response from the Rayleigh point of view enables the BCZT response to be compared with other compounds. Comparing the Rayleigh coefficient between BCZT, $\alpha_{BCZT}^{\varepsilon}$= 43500 mm/kV, PNZT, $\alpha_{PNZT}^{\varepsilon}$= 2600 mm/kV, and KNL-NTS, $\alpha_{KNL-NTS}^{\varepsilon}$= 1300 mm/kV, the colossal nonlinear dielectric response of the BCZT is proven. The value of α^{ε} for BCZT is one order of magnitude higher than the other studied systems, which suggests extensive instabilities of the functional properties in this system. Fig. 5(b) shows the m_{ε} value for BCZT, which is comparable with the value of a soft PZT [9]. According to the Rayleigh model, this result indicates that the major contribution to the nonlinear response in BCZT is the irreversible motion of domain walls. Understanding and controlling the physical phenomena related to the domain wall motion will be fundamental for the use of this compound in real applications.

The colossal nonlinear dielectric response displayed in BCZT piezoceramics may also be illustrated by taking into account the coercive field value of this compound when compared with other systems such as PNZT and KNL-NTS (Fig. 5(c)). The nonlinear dielectric characterization is usually performed at sub-switching electric fields (i.e., $E_0 < \frac{E_C}{2}$) to avoid nucleation or coalescence of the ferroelectric domains. Variations on the permittivity start increasing at applied electric fields one order of magnitude below the coercive field ($E_0 < 0.1E_C$) for all studied materials, as may be observed in Fig. 5(a). However, the extremely low value of the coercive field ($E_C \approx 0.2$ kV/mm) in the BCZT implies that even at amplitudes of the applied electric fields as low as $E_0 = 20$ V/mm the nonlinear phenomenon is observable.

Fig. 6 shows the nonlinear piezoelectric response of the BCZT. The variation of the piezoelectric coefficient, d_{33}^{NL}, with the amplitude of the applied dynamical stress, T_0, is shown in Fig. 6(a) for different uniaxial compressive pre-stress, T_{DC}. At the lowest pre-stress, T_{DC}= 10 MPa, and a relatively small value of dynamical stress, $T_0 \approx$ 5 MPa, the d_{33}^{NL} doubles the initial value, exhibiting a high nonlinear piezoelectric response. However, the nonlinear piezoelectric response decreases with the increase in T_{DC}. Similar behaviour has been reported in PNZT [26], although the variation of the piezoelectric coefficient reported for PNZT is noticeably lower than the variation observed in BCZT. The unusual variation of the longitudinal piezoelectric coefficient in BCZT at relatively small values of external mechanical stimulus produces high instability of the piezoelectric response in this system.

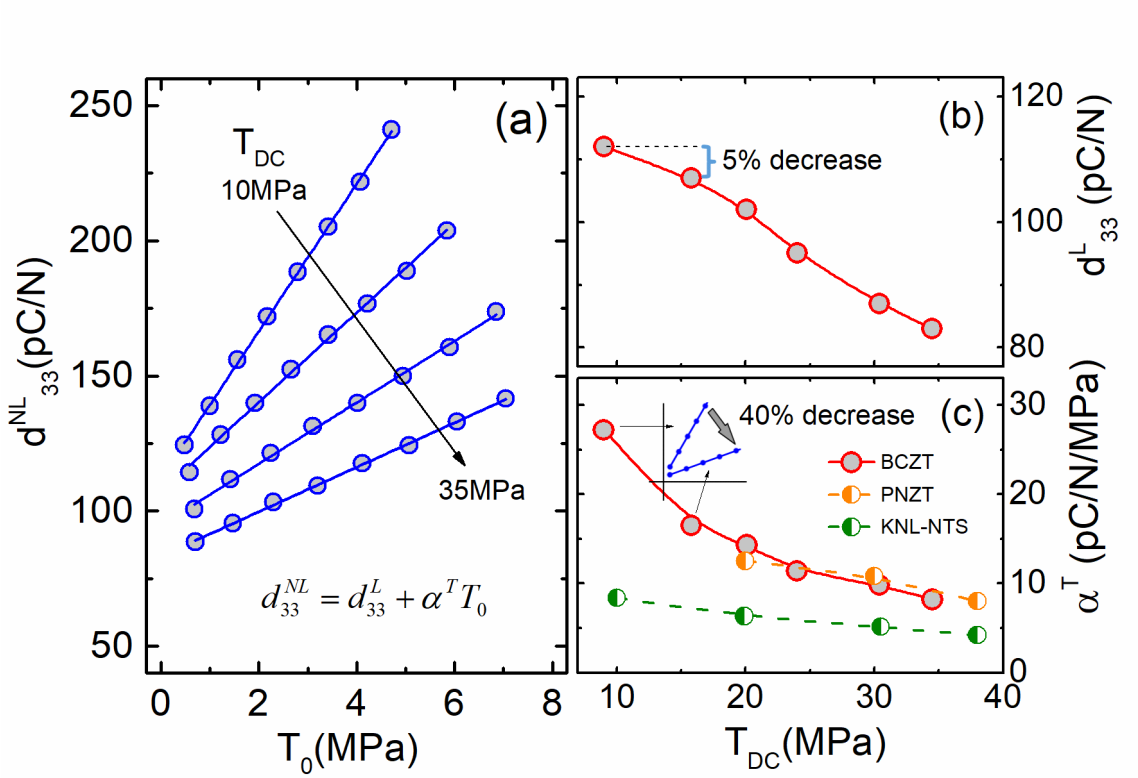

Fig. 6. (a) Direct piezoelectric coefficient d_{33} of BCZT as a function of the amplitude of the applied dynamical stress (T_0) for several uniaxial compressive pre-stress (T_{DC}), at 10 Hz and at room temperature. Panel (b) shows the direct piezoelectric coefficient d_{330} at zero-stress amplitude (T_0=0) as a function of T_{DC}. The slope α^T of the linear relation between the increment of the direct piezoelectric coefficient and T_0 is plotted in panel (c) as a function of T_{DC}.

The nonlinear piezoelectric response of soft piezoelectric materials, which is similar to the nonlinear dielectric response, could be described by the Rayleigh model. According to this model, the value of the piezoelectric coefficient depends linearly on the amplitude of the applied dynamical stress, and is expressed by:

$$d_{33}^{NL}(T_0) = d_{33}^{L} + \alpha^T T_0,$$

where d_{33}^{L} is the piezoelectric coefficient at $T_0 = 0$, which can be obtained by extrapolation of the d_{33}^{NL} versus T_0 curve. The Rayleigh coefficient α^T, similar to α^{ε}, quantifies the nonlinear piezoelectric response. Unlike the dielectric response, the nonlinear piezoelectric response of BCZT appears to fulfil the Rayleigh model, as shown recently in BCZT single crystals [33]. The d_{33}^{NL} values linearly increase with the increase in T_0 for all T_{DC}, as may be verified in Fig. 6(a). The decrease in the slope with the increase in T_{DC} indicates a decrease in the nonlinear behaviour, thereby leading to an enhancement of the functional properties stability.

A more useful analysis can be performed from the study of the linear piezoelectric coefficient, d_{33}^{L}, and the Rayleigh coefficient α^{T}, as a function of the applied uniaxial compressive pre-stress, T_{DC}. Figs. 6(b) and 6(c) show the d_{33}^{L} and α^{T} dependences with T_{DC}, respectively. The values of α^{T} for PNZT and KNL-NTS are plotted for comparison purposes. Both d_{33}^{L} and α^{T} decreases with the increase in T_{DC}. In a range of ΔT_{DC}= 25 MPa, the d_{33}^{L} drops by 30% from the initial value. A similar fall occurs in $\alpha_{BZT-BCT}^{T}$ over the same ΔT_{DC} range. On the other hand, neither α_{PNZT}^{T} nor $\alpha_{KNL-NTS}^{T}$ show significant changes in the whole T_{DC} range. Nevertheless, on approaching the highest T_{DC} value, all the Rayleigh coefficients tend toward the same value.

An interesting particularity arises from the analysis of the BCZT piezoelectric response with T_{DC}. The value of the longitudinal piezoelectric coefficient for an unclamped sample of BCZT is as high as ~410 pC/N (measured in a typical d_{33}-meter). However, when a moderate uniaxial compression stress is applied to the sample, a marked decrease in the piezoelectric response occurs; e.g., d_{33} drop to ~110 pC/N for a T_{DC}= 10 MPa (Fig. 6(b)). Nevertheless, the increase in T_{DC} leads to a decrease in α^{T} (Fig. 6(c)), promoting the stability of the piezoelectric properties. Note that for a typical work value of T_{DC}= 15 MPa, the 5% decrease in the d_{33}^{L} is much lower than the 40% decrease in the α^{T}. Although the functional response decreases, the faster approach to the enhancement of the property stability is a remarkable feature from the point of view of applications.

Table 2. Some room temperature properties and Rayleigh coefficients of the BCZT summarizing the comparison with the KNL-NTS and PNZT compounds.

	BCZT	KNL-NTS	PNZT
d_{33} (pC/N)	410	270	255
d_{31} (pC/N)	42	65	55
s^{E}_{11} (pm/Pa)	13	10	11
ε^{T}_{33}	1820	980	1450
k_{31}	0.27	0.22	0.26
α^{ε} (mm/kV)	43500	1300	2600
α^{T} (pC/N/MPa)*	14.3	6.3	12.5

*Values for a uniaxial pre-stress of 20 MPa

The observed nonlinear piezoelectric behavior of BCZT is in agreement with previous results [26] from a qualitative point of view, which can be explained by two different mechanisms. First, the clamp of the ferroelectric-ferroelastic domain walls as consequence of the external uniaxial pre-stress could substantially reduce both the reversible and the

irreversible domain walls motion. A second mechanism could be associated with the existence of a stress-driven phase transformation moving the BCZT out of the MPB region. Table 2 summarizes Rayleigh coefficients and some room temperature properties of BCZT, KNL-NTS and PNZT for a direct quantitative comparison between these compounds.

4. Conclusion

The variation in the dielectric and piezoelectric response with the applied external stimuli show a colossal nonlinear behavior in the BCZT, leading to a huge instability of the functional properties. These instabilities manifest at considerably low amplitudes of the applied electric field or dynamical stress, thereby compromising the use of this material for actuator applications. The Rayleigh model is used to study quantitatively the nonlinear response. The results show that a control of the nonlinear behavior of this system seems to be mandatory, for instance, through domain engineering processes. Considering that the dynamic of the domain walls is sensitive to the concentration and nature of point defects, further studies must be performed to achieve an enhancement of the functional properties stability.

Acknowledgments

This work is supported by the MINECO (Spanish Government) project ESP2015-72277-EXP. The authors thank Guillermo Gallego his contribution to the low-temperature measurements. A. Reyes-Montero gratefully thanks CONACyT-México for providing a PhD scholarship, as well as Federico González and LDRX (T-128) UAM-I for XRD measurements. M. E. Villafuerte-Castrejón acknowledges CIC-UNAM and PAPIIT UNAM (IN109018) for the academic exchange support and economic funding, respectively. L. Pardo acknowledges MINECO (MAT2017-86168-R) for its financial support.

References

[1] J. N. Gordon, A. Taylor, P. N. Bennett, Lead poisoning: case studies, Br. J. Clin. Pharmacol. 53 (2002) 451–458.

[2] Y. Saito, H. Takao, T. Tani, T. Nonoyama, K. Takatori, T. Homma, T. Nagaya, M. Nakamura, Lead-free piezoceramics, Nature 432 (2004) 84–87.

[3] S. Priya, S. Nahm (Eds.), Lead-Free Piezoelectrics, Springer, New York, 2012.

[4] M. E. Villafuerte-Castrejón, E. Morán, A. Reyes-Montero, R. Vivar-Ocampo, J. A. Peña-Jiménez, S. O. Rea-López, L. Pardo, Towards lead-free piezoceramics: facing a synthesis challenge, Materials 9 (2016) 21.

[5] J. Rödel, K. Webber, R. Dittmer, W. Jo, M. Kimura, D. Damjanovic, Transfering lead-free piezoelectric ceramics into application, J. Eur. Ceram. Soc. 35 (2015) 1659.

[6] D. Damjanovic, A morphotropic phase boundary system based on polarization rotation and polarization extension, Appl. Phys. Lett. 97 (2010) 062906.

[7] D. A. Ochoa, G. Esteves, J. L. Jones, F. Rubio-Marcos, J. F. Fernández, J. E. García, Extrinsic response enhancement at the polymorphic phase boundary in piezoelectric materials, Appl. Phys. Lett. 108 (2016) 142901.

[8] Q. M. Zhang, H. Wang, N. Kim, L. E. Cross, Direct evaluation of domain wall and intrinsic contributions to the dielectric and piezoelectric response and their temperature dependence on lead zirconate titanate, J. Appl. Phys. 75 (1994) 454-459.

[9] J. E. García, R. Pérez, D. A. Ochoa, A. Albareda, M. H. Lente, J. A. Eiras, Evaluation of domain wall motion in lead zirconate titanate ceramics by nonlinear response measurements, J. Appl. Phys. 103 (2008) 054108.

[10] M. Acosta, N. Novak, V. Rojas, S. Patel, R. Vaish, J. Koruza, G. A. Rossetti, J. Rödel, $BaTiO_3$-based piezoelectrics: Fundamentals, current status, and perspectives, Appl. Phys. Rev. 4 (2017) 041305.

[11] W. Liu, X. Ren, Large piezoelectric effect in Pb-free ceramics, Phys. Rev. Lett. 103 (2009) 257602.

[12] L. Zhang, M. Zhang, L. Wang, C. Zhou, Z. Zhang, Y. Yao, L. Zhang, D. Xue, X. Lou, X. Ren, Phase transitions and the piezoelectricity around morphotropic phase boundary in $Ba(Zr_{0.2}Ti_{0.8})O_3$-$x(Ba_{0.7}Ca_{0.3})TiO_3$ lead-free solid solution, Appl. Phys. Lett. 105 (2014) 162908.

[13] D. Xue, Y. Zhou, H. Bao, C. Zhou, J. Gao, X. Ren, Elastic, piezoelectric, and dielectric properties of $Ba(Zr_{0.2}Ti_{0.8})O_3$-$50(Ba_{0.7}Ca_{0.3})TiO_3$ Pb-free ceramic at the morphotropic phase boundary. J. Appl. Phys. 109 (2011) 054110.

[14] L. Bellaiche, A. Garcia, D. Vanderbilt, Finite-temperature properties of $Pb(Zr_{1-x}Ti_x)O_3$ alloys from first principles, Phys. Rev. Lett. 84 (2000) 5427.

[15] T. Iamsasri, G. Tutuncu, C. Uthaisar, S. Pojprapai, J. L. Jones, Analysis methods for characterizing ferroelectric/ferroelastic domain reorientation in orthorhombic perovskite materials and application to Li-doped $Na_{0.5}K_{0.5}NbO_3$, J. Mater. Sci. 48 (2013) 6905-6910.

[16] R. Yuan, D. Xue, Y. Zhou, X. Ding, J. Sun, D. Xue, Ferroelectric, elastic, piezoelectric, and dielectric properties of $Ba(Ti_{0.7}Zr_{0.3})O_3$-$x(Ba_{0.82}Ca_{0.18})TiO_3$ Pb-free ceramics, J. Appl. Phys. 122 (2017) 044105.

[17] J. Gao, X. Hu, L. Zhang, F. Li, L. Zhang, Y. Wang, Y. Hao, L. Zhong, X. Ren. Major contributor to the large piezoelectric response in $(1-x)Ba(Zr_{0.2}Ti_{0.8})O_3-x(Ba_{0.7}Ca_{0.3})TiO_3$ ceramics: Domain wall motion, Appl. Phys. Lett. 104 (2014) 252909.

[18] Y. Zhang, L. Tang, H. Tian, J. Wang, W. Cao, Z. Zhang, Determination of temperature dependence of full matrix material constants of PZT-8 piezoceramics using only one sample, J. Alloys Compd. 714 (2017) 20-25.

[19] Y. Zhang, Z. Chen, W. Cao, Z. Zhang, Temperature and frequency dependence of the coercive field of $0.71PbMb_{1/3}Nb_{2/3}O_3–0.29PbTiO_3$ relaxor-based ferroelectric single crystal, Appl. Phys. Lett. 111 (2017) 172902.

[20] A. Reyes-Montero, L. Pardo, R. López-Juárez, A. M. González, S. O. Rea-López, M. P. Cruz, M. E. Villafuerte-Castrejón, Sub-10μm grain size, $Ba_{1-x}Ca_xTi_{0.9}Zr_{0.1}O_3$ (x=0.10 and x=0.15) piezoceramics processed using a reduced thermal treatment, Smart Mater. Struct. 24 (2015) 065033.

[21] F. Rubio-Marcos, P. Ochoa, J. F. Fernandez, Sintering and properties of lead-free $(K,Na,Li)(Nb,Ta,Sb)O_3$ ceramics, J. Eur. Ceram. Soc., 27 (2007) 4125–4129.

[22] F. Benabdallah, A. Simon, H. Khemakhem, C. Elissalde, M. Maglione, Linking large piezoelectric coefficients to highly flexible polarization of lead free $BaTiO_3$-$CaTiO_3$-$BaZrO_3$ ceramics, J. Appl. Phys. 109 (2011) 124116.

[23] Publication and proposed revision of ANSI/IEEE Standard 176-1987 "ANSI/IEEE Standard on Piezoelectricity", IEEE Trans. Ultrason. Ferroelectr. Freq. Control 43 (1996) 717–772.

[24] D. A. Ochoa, J. E. Garcia, R. Perez, A. Albareda, Influence of extrinsic contribution on the macroscopic properties of hard and soft lead zirconate titanate ceramics, IEEE Trans. Ultrason. Ferroelectr. Freq. Control 55 (2008) 2732–2736.

[25] J. E. García, R. Pérez, A. Albareda, High electric field measurement of dielectric constant and losses of ferroelectric ceramics, J. Phys. D. Appl. Phys. 34 (2001) 3279.

[26] D. A. Ochoa, J. E. García, I. Tamayo, V. Gomis, D. Damjanovic, and R. Pérez, Effect of uniaxial compressive stress on dielectric and piezoelectric responses in lead zirconate titanate based ceramics, J. Am. Ceram. Soc. 95 (2012) 1656–1660.

[27] A. Reyes-Montero, F. Rubio-Marcos, L. Pardo, A. Del Campo, R. López-Juárez, M. E. Villafuerte-Castrejón, Electric field effect on the microstructure and properties of $Ba_{0.9}Ca_{0.1}Ti_{0.9}Zr_{0.1}O_3$ (BCTZ) lead-free ceramics, J. Mater. Chem. A 6 (2018) 5419-5429.

[28] D.A. Ochoa, J.E. García, R. Perez, V. Gomis, A. Albareda, F. Rubio-Marcos, J.F. Fernandez, Extrinsic contribution and non-linear response in lead-free KNN-modified piezoceramics, J. Phys. D: Appl. Phys. 42 (2009) 025402.

[29] H. Fu, R. E. Cohen, Polarization rotation mechanism for ultrahigh electromechanical response in single-crystal piezoelectrics, Nature 403 (2000) 281-283.

[30] D. Damjanovic, M. Demartin, The Rayleigh law in piezoelectric ceramics, J. Phys. D. Appl. Phys. 29 (1999) 2057–2060.

[31] D. Zhan, Q. Xu, D.-P. Huang, H.-X. Liu, W. Chen, F. Zhang, Dielectric nonlinearity and electric breakdown behaviors of $Ba_{0.95}Ca_{0.05}Zr_{0.3}Ti_{0.7}O_3$ ceramics for energy storage utilizations, J. Alloys Compd. 682 (2016) 594-600.

[32] J. E. Garcia, D. A. Ochoa, V. Gomis, J. A. Eiras, R. Pérez, Evidence of temperature dependent domain wall dynamics in hard lead zirconate titanate piezoceramics, J. Appl. Phys. 112 (2012) 014113.

[33] D. Liu, J. Shim, Y. Sun, Q. Li, Q. Yan, Growth of Ca, Zr co-doped $BaTiO_3$ lead-free ferroelectric single crystal and its room temperature piezoelectricity, AIP Adv. 7 (2017) 095311.